

Charge doping induced thermal switches with a high switching ratio in monolayer MoS_2

Chen Gui(桂琛), Zhi-Fu Duan(段志福), Chang-Hao Ding(丁长浩), Hao Chen(陈浩), Yuan Yao(姚远), Nan-Nan Luo(罗南南), Jiang Zeng(曾犟), Li-Ming Tang(唐黎明), and Ke-Qiu Chen(陈克求)

Citatio: Chin. Phys. B, 2025, 34 (**9**): 097401. DOI: 10.1088/1674-1056/add907
http://cpb.iphy.ac.cn; http://iopscience.iop.org/cpb

What follows is a list of articles you may be interested in

Phonon resonance modulation in weak van der Waals heterostructures: Controlling thermal transport in graphene—silicon nanoparticle systems

Yi Li(李毅), Yinong Liu(刘一浓), and Shiqian Hu(胡世谦)
Chin. Phys. B, 2024, 33 (**4**): 047401. DOI: 10.1088/1674-1056/ad1501

Ultralow-temperature heat transport study of noncentrosymmetric superconductor CaPtAs

Yimin Wan(万一民), Erjian Cheng(程二建), Yuxin Chen(陈宇鑫), Chengcheng Zhao(赵成成), Chengpeng Tu(涂成鹏), Dongzhe Dai(戴东喆), Xiaofan Yang(杨小帆), Lu Xin(辛路), Wu Xie(谢武), Huiqiu Yuan(袁辉球), and Shiyan Li(李世燕)
Chin. Phys. B, 2023, 32 (**12**): 127403. DOI: 10.1088/1674-1056/ad02e9

Advances in thermoelectric $(GeTe)_x(AgSbTe_2)_{100-x}$

Hongxia Liu(刘虹霞), Xinyue Zhang(张馨月), Wen Li(李文), and Yanzhong Pei(裴艳中)
Chin. Phys. B, 2022, 31 (**4**): 047401. DOI: 10.1088/1674-1056/ac3cae

Two-dimensional square-Au_2S monolayer: A promising thermoelectric material with ultralow lattice thermal conductivity and high power factor

Wei Zhang(张伟), Xiao-Qiang Zhang(张晓强), Lei Liu(刘蕾), Zhao-Qi Wang(王朝棋), and Zhi-Guo Li(李治国)
Chin. Phys. B, 2021, 30 (**7**): 077405. DOI: 10.1088/1674-1056/abe115

Fabrication and characterization of Al-Mn superconducting films for applications in TES bolometers

Qing Yu(余晴), Yi-Fei Zhang(张翼飞), Chang-Hao Zhao(赵昌昊), Kai-Yong He(何楷泳), Ru-Tian Huang(黄汝田), Yong-Cheng He(何永成), Xin-Yu Wu(吴歆宇), Jian-She Liu(刘建设), and Wei Chen(陈炜)
Chin. Phys. B, 2021, 30 (**7**): 077402. DOI: 10.1088/1674-1056/abe0c6

SPECIAL TOPIC — Heat conduction and its related interdisciplinary areas

Charge doping induced thermal switches with a high switching ratio in monolayer MoS_2

Chen Gui(桂琛), Zhi-Fu Duan(段志福), Chang-Hao Ding(丁长浩), Hao Chen(陈浩), Yuan Yao(姚远), Nan-Nan Luo(罗南南)†, Jiang Zeng(曾犟), Li-Ming Tang(唐黎明), and Ke-Qiu Chen(陈克求)‡

Department of Physics, School of Physics and Electronics, Hunan University, Changsha 410082, *China*

(Received 15 March 2025; revised manuscript received 30 April 2025; accepted manuscript online 15 May 2025)

The thermal switch plays a crucial role in regulating system temperature, protecting devices from overheating, and improving energy efficiency. Achieving a high thermal switching ratio is essential for its practical application. In this study, by utilizing first-principles calculations and semi-classical Boltzmann transport theory, it is found that hole doping with an experimentally achievable concentration of 1.83×10^{14} cm^{-2} can reduce the lattice thermal conductivity of monolayer MoS_2 from 151.79 W·m^{-1}·K^{-1} to 12.19 W·m^{-1}·K^{-1}, achieving a high thermal switching ratio of 12.5. The achieved switching ratio significantly surpasses previously reported values, including those achieved by extreme strain methods. This phenomenon mainly arises from the enhanced lattice anharmonicity, which is primarily contributed by the S atoms. These results indicate that hole doping is an effective method for tuning the lattice thermal conductivity of materials, and demonstrate that monolayer MoS_2 is a potential candidate material for thermal switches.

Keywords: thermal switching ratio, thermal conductivity, anharmonicity, two-dimensional material

PACS: 74.25.Kc, 66.70.–f, 65.80.–g, 74.25.fc

DOI: 10.1088/1674-1056/add907 **CSTR:** 32038.14.CPB.add907

1. Introduction

A thermal switch is a device that can actively regulate heat transfer between the "on" and "off" states by applying external stimuli, such as electric fields, magnetic fields and pressure.[1–7] It holds significant promise for applications in efficient thermal management, power system optimization, electronic device protection, and intelligent temperature control, owing to its ability to dynamically modulate heat flow.[8–10] Key performance metrics for thermal switches include the thermal switching ratio (λ), response time and cyclic stability.[11] Compared to liquid metal thermal switches, which suffer from material instability, and mechanical thermal switches, which are prone to wear, solid-state thermal switches have garnered widespread attention. By leveraging the intrinsic properties of materials to regulate lattice thermal conductivity (κ_l), solid-state thermal switches eliminate the need for moving parts and offer a more stable and reliable structure.[8,12] For example, $HoMnO_3$ can modulate κ_l through magnetic field application, with thermal conductivity varying from 1 W·m^{-1}·K^{-1} to 0.05 W·m^{-1}·K^{-1}, achieving a thermal switching ratio of up to 20.[13] Similarly, NaCl exhibits a thermal switching ratio of 1.67, with thermal conductivity transitioning from 30.1 W·m^{-1}·K^{-1} to 18.0 W·m^{-1}·K^{-1} via a B1–B2 phase transition.[14]

Two-dimensional (2D) materials, with their atomic-scale thickness, excellent mechanical, electrical, and optical properties, present a promising avenue for achieving high thermal switching ratios.[13,15–26] For example, antiferroelectric thin films like $PbZrO_3$ have demonstrated high thermal switching rates ($\lambda > 2.2$) and rapid response times ($t < 150$ ns) through electric field-driven phase transitions.[27] Theoretical studies also predict that applying 2% biaxial strain can increase the κ_l of monolayer BS from 0.11 W·m^{-1}·K^{-1} to 34.5 W·m^{-1}·K^{-1}.[28] As a representative 2D semiconductor material, MoS_2 has attracted extensive attention due to its unique physicochemical properties.[29–33] Recent studies have demonstrated that the thermal conductivity of MoS_2 can be significantly modulated through extreme strain, defect-strain synergy, and electrochemical intercalation, achieving thermal switching ratios of 1.5, 6.3, and 2.3 along the in-plane direction, respectively.[3,34,35] However, the above modulation methods, such as magnetic fields, phase transitions, and strain, while capable of achieving high thermal switching ratios and fast response times, often require extreme operating conditions, suffer from irreversibility, or entail high energy consumption.[13,34,36] Moreover, charge doping by triboelectric effects exhibits high controllability, fast response, and excellent reversibility; moreover, it requires no mechanical parts, which has attracted considerable attention.[37,38] Therefore, identifying routinely reversible modulation mechanisms capable of achieving high thermal switching ratios under practical conditions in MoS_2 is of critical importance.

†Corresponding author. E-mail: luonn@hnu.edu.cn

‡Corresponding author. E-mail: keqiuchen@hnu.edu.cn

© 2025 Chinese Physical Society and IOP Publishing Ltd. All rights, including for text and data mining, AI training, and similar technologies, are reserved.

In this work, we demonstrate that hole doping serves as an effective strategy for achieving high thermal switching ratios in monolayer MoS_2 (ML-MoS_2). By integrating first-principles calculations with semi-classical Boltzmann transport theory, we systematically investigate the doping-concentration-dependent lattice dynamics and phonon scattering mechanisms. At an experimentally achievable hole concentration of 1.83×10^{14} cm^{-2}, κ_l of ML-MoS_2 is dramatically reduced from 151.79 W·m^{-1}·K^{-1} to 12.19 W·m^{-1}·K^{-1}, yielding a remarkable thermal switching ratio of 12.5. This reduction is attributed to doping-enhanced lattice anharmonicity, predominantly governed by the softened vibrational modes of sulfur atoms. Our findings not only highlight hole doping ML-MoS_2 as a promising candidate for high-performance thermal switches but also provide a general framework for tailoring thermal transport in 2D materials via carrier-mediated phonon engineering.

2. Computational method

The κ_l and phonon properties of ML-MoS_2 are obtained by combining density-functional theory (DFT) calculations with the phonon Boltzmann transport equation. The DFT calculations are carried out using the Vienna *ab initio* simulation package (VASP), and the exchange–correlation potentials are obtained using the Perdew–Burke–Ernzerhof (PBE) generalized gradient approximation.[39–42] The out-of-plane cell length is set as 25 Å to prevent spurious interactions between the 2D sheet and its periodic images, and the energy cutoff of the plane wave function is set to 400 eV. The structure is optimized with an energy convergence criterion of 10^{-7} eV and a force convergence criterion of 10^{-4} eV/Å. A Γ-centered k-point mesh of $12 \times 12 \times 1$ is utilized for sampling in the Brillouin zone. The calculations of second-order and third-order interatomic force constants (IFCs) are performed using the PHONOPY and Thirdorder packages.[43] The thermal transport properties are obtained using the ShengBTE software package.[44] The calculation flowchart has been added to the supporting information, as shown in Fig. S1. The tenth nearest neighbor is chosen as the cutoff radius to ensure convergence of the third-order IFC calculations. A $50 \times 50 \times 1$ q-grid and a smearing parameter of 1.0 are employed to ensure the convergence of the ShengBTE calculations. The details of the convergence tests are provided in Fig. S2 of the supporting information.

3. Results and discussion

3.1. Structure and stability

As shown in Fig. 1(a), the crystal structure of ML-MoS_2 consists of a layer of Mo atoms sandwiched between two layers of S atoms, forming a typical hexagonal crystal structure. The relaxed lattice constant is 3.180 Å, consistent with previous results.[37,45] The phonon spectra of ML-MoS_2 in the neutral state (n_0), with hole doping concentrations of 4.57×10^{13} cm^{-2} (n_1) and 1.83×10^{14} cm^{-2} (n_2), are shown in Figs. 1(b)–1(d), respectively. The absence of imaginary frequencies in all three phonon spectra confirms that MoS_2 remains structurally stable in both its neutral state and under hole doping. In addition, the in-plane longitudinal acoustic (LA) mode exhibits softening near the high-symmetry point K as the hole concentration increases. The phonon frequency of the LA mode at the high-symmetry point K decreases from 6.91 THz to 5.72 THz, reducing the gap between the LA and TA modes from 1.28 THz to 0.25 THz. This suggests that the strength of phonon–phonon scattering may increase with increasing hole concentration, potentially leading to a decrease in κ_l.

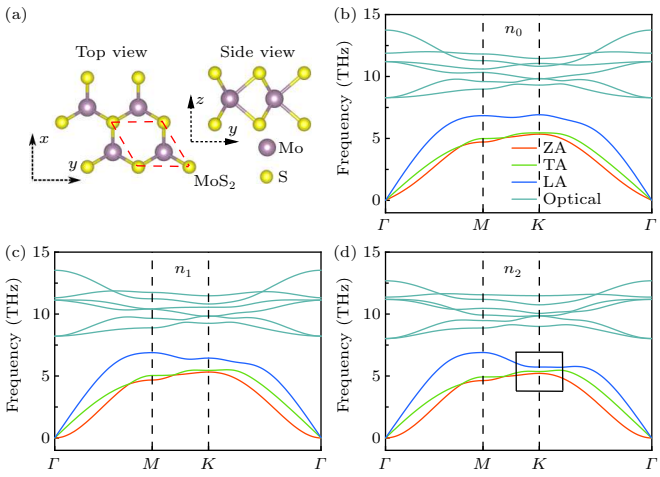


Fig. 1. (a) Top and side views of the lattice structure of monolayer MoS_2. The red dashed parallelogram represents the unit cell. (b)–(d) Phonon spectra of monolayer MoS_2 in the neutral state (n_0), with a hole doping concentration of 4.57×10^{13} cm^{-2} (n_1), and 1.83×10^{14} cm^{-2} (n_2), respectively. The flexural (ZA), transverse (TA), and longitudinal (LA) acoustic modes are represented in red, green, and blue, respectively. In panel (d), the dashed black square highlights the region of softening.

3.2. Thermal transport properties

Figure 2(a) shows the variation of κ_l as a function of temperature under different hole doping conditions. At room temperature (300 K), the calculated κ_l is 151.79 W·m^{-1}·K^{-1} in the neutral state, which shows good agreement with the experimentally measured values of 85–112 W·m^{-1}·K^{-1} and 84 ± 17 W·m^{-1}·K^{-1}.[46,47] Additionally, this result is consistent with several theoretical predictions, which report values of 138 W·m^{-1}·K^{-1} and 154.3 W·m^{-1}·K^{-1}.[48,49] The close agreement between the obtained results and previous experimental and theoretical values underscores the reliability of the calculation method employed. The results reveal that κ_l decreases with increasing hole concentration, indicating that higher doping levels suppress thermal conductivity. Specifically, κ_l reduces to 94.62 W·m^{-1}·K^{-1} and 12.19 W·m^{-1}·K^{-1} at hole concentrations of n_1 and n_2, respectively, at 300 K. This

indicates that at the experimentally achievable doping concentration (n_2), a high thermal switching ratio of 12.5 is obtained. It is worth noting that electron–phonon scattering, not considered in the present work, could further suppress κ_l at high doping levels, thereby leading to an even greater switching ratio.[50] Compared to the thermal switching ratios of 1.5, 6.3, and 2.2 for strain, lithium-ion doping, and strain-synergistic defect-modulated MoS_2 thermal conductivities, the thermal switching ratio achieved by hole doping in this work is significantly higher. Furthermore, recent experiments and theoretical work have shown that controllable doping can be induced in MoS_2 through triboelectric effects, highlighting the feasibility of modulating thermal transport properties in this material through hole doping.[37,38] Compared to methods based on electrochemical lithium intercalation and extreme strain engineering,[3,35] the thermal switching ratio achieved here is significantly higher, while the doping-based approach is also more convenient.

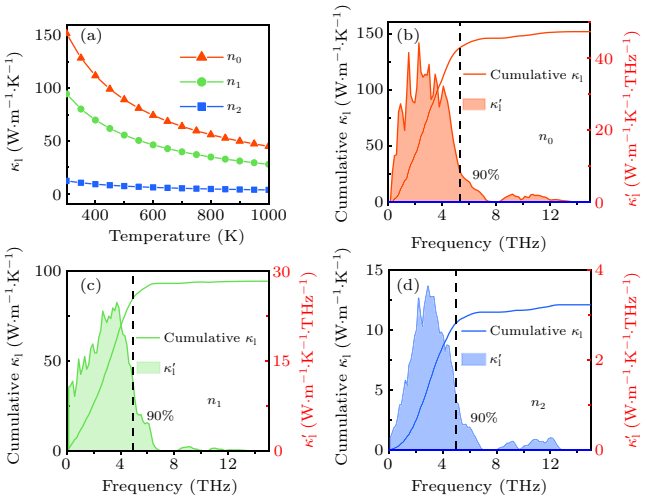


Fig. 2. (a) The lattice thermal conductivity, κ_l, as a function of temperature for the neutral state (n_0) and hole doping concentrations n_1 and n_2. At 300 K, the cumulative κ_l and the derivative of the cumulative κ_l, denoted κ_l', for n_0 (b), n_1 (c), and n_2 (d).

To understand the physical mechanism behind the significant reduction in κ_l under hole doping, we first analyze the frequency-resolved phonon contributions and their cumulative impact on κ_l as a function of frequency. Using the 300 K case as an example, Figs. 2(b)–2(d) reveal that κ_l is primarily governed by acoustic phonon interactions in both neutral and hole-doped systems. Specifically, the cumulative κ_l reaches 90% at frequencies of 5.29 THz, 4.92 THz, and 5.01 THz for the neutral state, hole concentration n_1 and n_2, respectively.

Next, focusing on low-frequency acoustic phonons, we conduct a detailed analysis of the parameters influencing κ_l, including the phonon group velocity v_λ and the phonon lifetime τ_λ. As shown in Fig. S3(a) of the supporting information, the change in v_λ remains minimal with increasing hole doping concentration. Thus, the variation in v_λ under hole doping is unlikely to be the main cause of the significant reduction in κ_l. In contrast, the overall decrease in τ_λ, as shown in Figs. 3(a)–3(c), is more pronounced, making it the dominant factor in the reduction of κ_l. τ_λ is mainly determined by the phonon-phonon scattering strength and the weighted phonon scattering phase space (W). The former can be inferred from the Grüneisen parameter ($\gamma_\lambda(q)$)

$$\gamma_\lambda(q) = -\frac{V}{\omega_\lambda(q)}\frac{\partial\omega_\lambda(q)}{\partial V}, \tag{1}$$

where $\omega_\lambda(q)$ is the frequency of the λ-th vibrational mode at wave vector q, and V is the volume of the system. W is expressed as

$$W_\lambda^{\pm} = \frac{1}{2N}\sum_{\lambda',\lambda''}\left\{\begin{matrix}2(f_{\lambda'}-f_{\lambda''})\\ f_{\lambda'}+f_{\lambda''}+1\end{matrix}\right\}\frac{\delta(\omega_\lambda\pm\omega_{\lambda'}-\omega_{\lambda''})}{\omega_\lambda\omega_{\lambda'}\omega_{\lambda''}}, \tag{2}$$

where $f_{\lambda'}$ and $f_{\lambda''}$ are the Bose–Einstein occupation numbers for phonon modes λ' and λ'', respectively. $\delta(\omega_\lambda\pm\omega_{\lambda'}-\omega_{\lambda''})$ enforces energy conservation for absorption (+) and emission (−) processes.

As shown in Fig. S3(b) of the supporting information, W remains nearly unchanged under hole doping, while the variation in γ is significant, as shown in Figs. 3(d)–3(f). Therefore, the dominant factor affecting τ_λ is γ. The magnitude of γ is directly related to the strength of the anharmonic effects. The larger $|\gamma|$ is, the stronger the anharmonicity of the material, and the shorter the phonon lifetime. Here, as the hole doping concentration increases, $|\gamma|$ in the low-frequency region increases, leading to a reduction in the phonon lifetime of the material. Specifically, in contrast to the LA and TA modes, the contributions of the ZA mode to γ exhibit fewer variations with increasing hole concentration. Consequently, its impact on the phonon lifetime remains relatively stable. Notably, at a hole concentration of n_2, the γ values from the LA and TA modes away from the Γ point are significantly higher than those at n_0 and n_1, leading to a pronounced reduction in the phonon lifetime at n_2. This increase in γ in the low-energy region may be attributed to the substantial softening of the LA mode near the K point for n_2.

Mean-squared displacement (MSD) analysis is used to investigate the origin of lattice anharmonicity. The MSD of atoms at finite temperatures, within the harmonic approximation, is expressed as[43,51]

$$\left\langle|u^\alpha(jl,t)|^2\right\rangle = \frac{\hbar}{2Nm_j}\sum_{\boldsymbol{q},\nu}\omega_\nu(\boldsymbol{q})^{-1} \times(1+2n_\nu(\boldsymbol{q},T))\,|e_\nu^\alpha(j,\boldsymbol{q})|^2, \tag{3}$$

where j and l are the labels for the j-th atomic position in the l-th unit cell, t is the time, T is the temperature, e is the polarization vector describing the polarization of the j-th atom along

the α-direction in the v-th branch of the vibrational mode with wave vector q, and $n_v(\boldsymbol{q},T)$ is the phonon population given by

$$n_v(\boldsymbol{q},T)=\frac{1}{\exp\left(\hbar\omega_v(\boldsymbol{q})/k_{\mathrm{B}}T\right)-1}, \tag{4}$$

where k_{B} is the Boltzmann constant. The higher the MSD value of an atom at the same temperature, the more anharmonic it is, which has been demonstrated both theoretically and experimentally.[52,53]

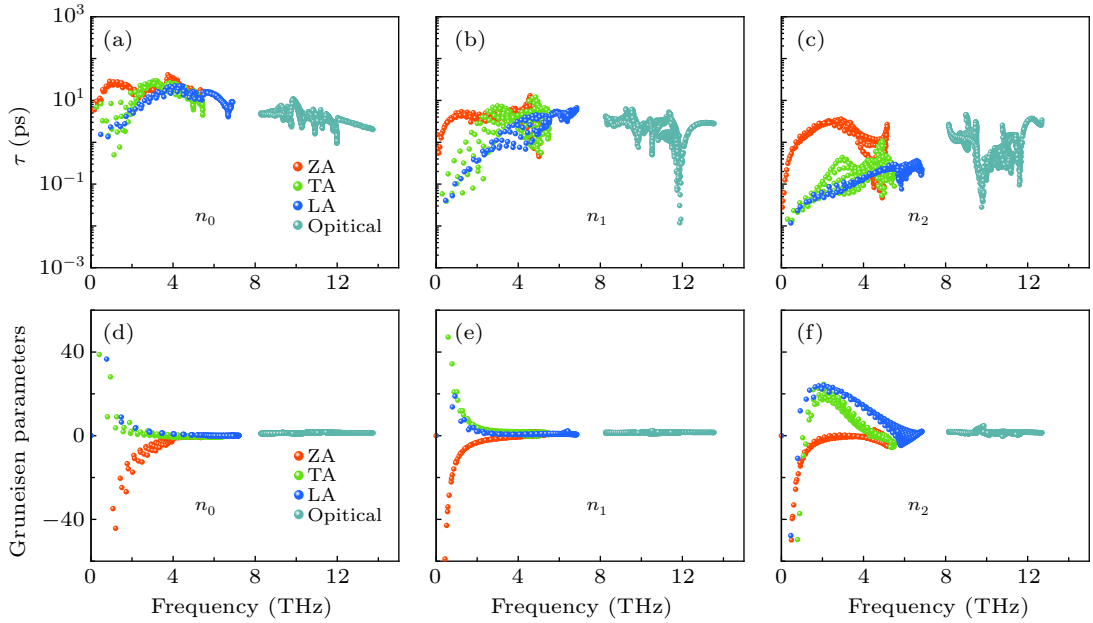


Fig. 3. Mode-resolved phonon lifetimes (a)–(c) and Grüneisen parameters (d)–(f) of ML-MoS_2 for the neutral state (n_0), and under hole doping with concentrations n_1 and n_2 at room temperature. Panels (a) and (d) correspond to the n_0 state; (b) and (e) correspond to the n_1 state; and (c) and (f) correspond to the n_2 state.

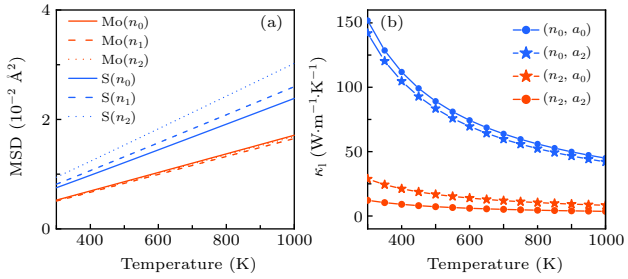


Fig. 4. (a) The temperature-dependent mean square displacement (MSD) of Mo and S atoms for the neutral state (n_0) and hole doping concentrations n_1 and n_2. (b) The lattice thermal conductivity, κ_l of ML-MoS_2 as a function of temperature under different conditions, where a_0 and a_2 represent the relaxed lattice constants for the n_0 and n_2 states, respectively.

It provides atomic-level insights into the evolution of lattice anharmonicity with doping concentration. As shown in Fig. 4(a), under neutral conditions, Mo atoms exhibit weaker anharmonicity compared to S atoms. As the doping concentration increases, the anharmonicity of Mo atoms remains nearly constant, whereas that of S atoms exhibits a significant enhancement. These results clearly demonstrate that the enhanced lattice anharmonicity at higher doping concentrations is predominantly caused by the dynamics of S atoms. The MSD results can be explained by the variation in the mechanical properties. The elastic constant decreases from 150.52 N/m to 138.92 N/m and 134.49 N/m as the doping concentration increases from n_0 to n_1 and n_2, respectively. The gradual decrease in the elastic constants indicates that the material becomes progressively softer. As a result, the MSD of the S atoms increases, leading to enhanced phonon anharmonicity. See the supporting information for more details of the calculation method of the elastic constant.

In the following analysis, we systematically investigate whether hole-doping-induced thermal conductivity reduction stems primarily from the doping itself or from doping-induced lattice constant variations. Using neutral and n_2-doped configurations as representative cases, it is found that doping modifies the lattice constant from $a_0 = 3.180$ Å to $a_2 = 3.185$ Å, corresponding to an increase of only 0.16%. As shown in Fig. 4(b), κ_l shows minimal variation when only the lattice constant is altered, either in neutral or doped systems. In contrast, maintaining a constant lattice while varying doping concentration leads to significant changes in thermal conductivity. These findings demonstrate that the reduction in thermal conductivity is predominantly attributed to the doping effect itself, with lattice constant variations playing only a minor role.

4. Conclusion

In conclusion, by combining first-principles calculations with Boltzmann transport theory, we reveal that hole doping significantly suppresses the lattice thermal conductivity (κ_l) of ML-MoS_2. At room temperature, the obtained κ_l of pristine ML-MoS_2 is 151.79 W·m^{-1}·K^{-1}, consistent with previous experimental and theoretical results. At an experimentally

achievable hole doping concentration of 1.83×10^{14} cm^{-2}, κ_l drops to 12.19 W·m^{-1}·K^{-1}, corresponding to a thermal switching ratio of 12.5. This switching ratio markedly surpasses previously reported values, including those achieved by extreme strain methods. The observed reduction in κ_l is primarily attributed to the enhanced lattice anharmonicity induced by hole doping, which is largely contributed by the S atoms. These findings highlight ML-MoS_2 as a promising candidate material for thermal switches and demonstrate that hole doping is an effective strategy to tune the thermal conductivity of materials.

For more details on the calculations, convergence tests, group velocity, and scattering phase space of ML-MoS_2 at room temperature for various hole doping concentrations, please refer to the supporting information.

Acknowledgment

This work was supported by the National Natural Science Foundation of China (Grant Nos. 12104145 and 12374040).

References

[1] Lu Q, Huberman S, Zhang H, Song Q, Wang J, Vardar G, Hunt A, Waluyo I, Chen G and Yildiz B 2020 *Nat. Mater.* **19** 655
[2] Hentrich R, Wolter A U B, Zotos X, Brenig W, Nowak D, Isaeva A, Doert T, Banerjee A, Lampen-Kelley P, Mandrus D G, Nagler S E, Sears J, Kim Y J, Büchner B and Hess C 2018 *Phys. Rev. Lett.* **120** 117204
[3] Meng X H, Pandey T, Jeong J, Fu S Y, Yang J, Chen K, Singh A, He F, Xu X C, Zhou J S, Hsieh W P, Singh A K, Lin J F and Wang Y G 2019 *Phys. Rev. Lett.* **122** 155901
[4] Pan H, Ding Z K, Zeng B W, Luo N N, Zeng J, Tang L M and Chen K Q 2023 *Phys. Rev. B* **107** 104303
[5] Pan H, Tang L M and Chen K Q 2022 *Phys. Rev. B* **105** 064401
[6] Jia J J, Li S C, Chen X and Shigesato Y 2024 *Adv. Funct. Mater.* **34** 2406667
[7] Lian M, Geng Y, Chen Y J, Chen Y and Lü J T 2024 *Phys. Rev. Lett.* **133** 116303
[8] Swoboda T, Klinar K, Yalamarthy A S, Kitanovski A and Rojo M M 2021 *Adv. Electron. Mater.* **7** 2170008
[9] Shin J, Sung J, Kang M, Xie X, Lee B, Lee K M, White T J, Leal C, Sottos N R, Braun P V and Cahill D G 2019 *Proc. Nat. Acad. Sci. USA* **116** 5973
[10] Hu P, Wang J, Zhang P, Wu F, Cheng Y, Wang J and Sun Z 2023 *Adv. Mater.* **35** 2207638
[11] Du T T, Xiong Z X, Delgado L, Liao W Z, Peoples J, Kantharaj R, Chowdhury P R, Marconnet A and Ruan X L 2021 *Nat. Commun.* **12** 4915
[12] Zheng R T, Gao J W, Wang J J and Chen G 2011 *Nat. Commun.* **2** 289
[13] Wang X M, Fan C, Zhao Z Y, Tao W, Liu X G, Ke W P, Zhao X and Sun X F 2010 *Phys. Rev. B* **82** 094405
[14] McGuire C, Sawchuk K and Kavner A 2018 *J. Appl. Phys.* **124** 115902
[15] Gu X K, Wei Y J, Yin X B, Li B W and Yang R G 2018 *Rev. Mod. Phys.* **90** 041002
[16] Kim S E, Mujid F, Rai A, Eriksson F, Suh J, Poddar P, Ray A, Park C, Fransson E, Zhong Y, Muller D A, Erhart P, Cahill D G and Park J 2021 *Nature* **597** 660
[17] He R, Wang D, Luo N N, Zeng J, Chen K Q and Tang L M 2023 *Phys. Rev. Lett.* **130** 046401
[18] Liu W, Ding Z K, Luo N, Zeng J, Tang L M and Chen K Q 2024 *Phys. Rev. B* **109** 115422
[19] Li Q Q, Liu W W, Ding Z K, Pan H, Cao X H, Xiao W H, Luo N N, Zeng J, Tang L M, Li B, Chen K Q and Duan X D 2023 *Appl. Phys. Lett.* **122** 121902
[20] Xiao W H, Yang K, D'Agosta R, Xu H R, Ouyang G, Zhou G, Chen K Q and Tang L M 2024 *Phys. Rev. B* **109** 115427
[21] Li Q Q, Duan Z F, Liu W W, Yang R, Li B and Chen K Q 2025 *Nano Res.* **18** 94907188
[22] Wang Y, Luo N, Zeng J, Tang L M and Chen K Q 2023 *Phys. Rev. B* **108** 054401
[23] Ding Z K, Zeng Y J, Liu W, Tang L M and Chen K Q 2024 *Adv. Funct. Mater.* **34** 2401684
[24] Duan Z F, Ding C H, Ding Z K, Xiao W H, Xie F, Luo N N, Zeng J, Tang L M and Chen K Q 2024 *Chin. Phys. B* **33** 087302
[25] Luo N, Zeng J, Tang L M and Chen K Q 2025 *Phys. Rev. B* **111** 125416
[26] Liu W, Ding Z K, Luo N, Zeng J, Tang L M and Chen K Q 2025 *Phys. Rev. B* **111** 115407
[27] Liu C H, Si Y Y, Zhang H, Wu C, Deng S Q, Dong Y Q, Li Y J, Zhuo M, Fan N B, Xu B, Lu P, Zhang L F, Lin X, Liu X J, Yang J K, Luo Z L, Das S, Bellaiche L, Chen Y F and Chen Z H 2023 *Science* **382** 1265
[28] Duan Z F, Ding Z K, Xie F, Zeng J, Tang L M, Luo N N and Chen K Q 2025 *Appl. Phys. Lett.* **126** 022205
[29] Sangwan V K, Lee H S, Bergeron H, Balla I, Beck M E, Chen K S and Hersam M C 2018 *Nature* **554** 500
[30] Radisavljevic B, Radenovic A, Brivio J, Giacometti V and Kis A 2011 *Nat. Nanotechnol.* **6** 147
[31] Yue Q, Kang J, Shao Z Z, Zhang X A, Chang S L, Wang G, Qin S Q and Li J B 2012 *Phys. Lett. A* **376** 1166
[32] Jia P Z, Zeng Y J, Wu D, Pan H, Cao X H, Zhou W X, Xie Z X, Zhang J X and Chen K Q 2020 *J. Phys.: Condens. Mat.* **32** 055302
[33] Wang J, Cao X H, Zeng Y J, Luo N N, Tang L M and Chen K Q 2023 *Appl. Surf. Sci.* **612** 155914
[34] Ding Z W, Pei Q X, Jiang J W and Zhang Y W 2015 *J. Phys. Chem. C* **119** 16358
[35] Zhu G H, Liu J, Zheng Q Y, Zhang R G, Li D Y, Banerjee D and Cahill D G 2016 *Nat. Commun.* **7** 13211
[36] Lin Y C, Dumcencon D O, Huang Y S and Suenaga K 2014 *Nat. Nanotechnol.* **9** 391
[37] Hedau B, Kang B C and Ha T J 2022 *ACS Nano* **16** 18355
[38] Gao H Q, Hu M A, Ding J F, Xia B L, Yuan G L, Sun H S, Xu Q H, Zhao S Y, Jiang Y W, Wu H, Yuan M, Li J H, Li B X, Zhao J, Rao D W and Xie Y N 2023 *Adv. Funct. Mater.* **33** 2213410
[39] Kresse and Furthmuller 1996 *Phys. Rev. B* **54** 11169
[40] Blochl 1994 *Phys. Rev. B* **50** 17953
[41] Perdew, Burke and Ernzerhof 1996 *Phys. Rev. Lett.* **77** 3865
[42] Li H, Tang Z, Fu J, Dong W H, Zou N, Gong X, Duan W and Xu Y 2024 *Phys. Rev. Lett.* **132** 096401
[43] Togo A 2023 *J. Phys. Soc. Jpn.* **92** 012001
[44] Li W, Carrete J, Katcho N A and Mingo N 2014 *Comput. Phys. Commun.* **185** 1747
[45] Ekuma C E, Najmaei S and Dubey M 2019 *Mater. Today Commun.* **19** 383
[46] Liu J, Choi G M and Cahill D G 2014 *J. Appl. Phys.* **116** 233107
[47] Zhang X, Sun D Z, Li Y L, Lee G H, Cui X, Chenet D, You Y M, Heinz T F and Hone J C 2015 *ACS Appl. Mater. Interfaces* **7** 25923
[48] Gu X K, Li B W and Yang R G 2016 *J. Appl. Phys.* **119** 085106
[49] Peng B, Ning Z Y, Zhang H, Shao H Z, Xu Y F, Ni G and Zhu H Y 2016 *J. Phys. Chem. C* **120** 29324
[50] Zhou J, Shin H D, Chen K, Song B, Duncan R A, Xu Q, Maznev A A, Nelson K A and Chen G 2020 *Nat. Commun.* **11** 6040
[51] Togo A and Tanaka I 2015 *Scr. Mater.* **108** 1
[52] Wu Y, Shi W, He C, Li J, Tang C and Ouyang T 2024 *Appl. Phys. Lett.* **124** 202203
[53] Lane N J, Vogel S C, Hug G, Togo A, Chaput L, Hultman L and Barsoum M W 2012 *Phys. Rev. B* **86** 214301